Supporting Information

Engineering of blended nanoparticle platform for delivery of mitochondria-acting therapeutics

Sean Marrache[a] and Shanta Dhar*[a,b]

[a]Nano Therapeutics Research Laboratory, Department of Chemistry, University of Georgia, Athens, GA 30602

[b]Department of Physiology and Pharmacology, University of Georgia, Athens, GA 30602

* To whom correspondence should be addressed.
E-mail: shanta@uga.edu

Corresponding Author:
Professor Shanta Dhar
Department of Chemistry, Room 679
University of Georgia
Athens, GA 30602
shanta@uga.edu, phone: 706-542-1012, fax: 706-542-9454

Materials.

All chemicals were received and used without further purification unless otherwise noted. PLGA-COOH of inherent viscosity of 0.18 dL/g was purchased from Lactel. HO-PEG-OH (MW 3350), 4-dimethylaminopyridine (DMAP), N,N'-dicyclohexylcarbodiimide (DCC), 2,4-DNP, curcumin, D-*α*-tocopherol succinate, LND, dexamethasone, 3-isobutyl-1-methylxanthine, and MTT were purchased from Sigma-Aldrich. Qdot 705 ITK amino PEG quantum dots, mitotracker green, and CellLight™ lysosomes-GFP were purchased from Invitrogen. Bicinchoninic acid (BCA) protein

assay and the mitochondria isolation kits were purchased from Thermo Scientific. AdipoRed™ adipogenesis assay reagent was purchased from Lonza. Amyloid *β*-protein fragment 25-35 was purchased from Sigma-Aldrich. Dynamic light scattering (DLS) measurements were carried out using a Malvern Zetasizer Nano ZS system. ^{1}H, ^{13}C, and ^{32}P NMR spectra were recorded on a 400 MHz Varian NMR spectrometer. Gel permeation chromatographic (GPC) analyses were performed on Shimadzu LC20-AD prominence liquid chromatographer equipped with a RI detector. Optical measurements were carried out on a NanoDrop 2000 spectrophotometer. HPLC analyses were made on an Agilent 1200 series instrument. TEM images were taken in a Tecnai 20 FEM microscope. Confocal images were recorded in a Nikon A1 confocal microscope. ICP-MS studies were performed on a VG PlasmaQuad 3 ICP mass spectrometer. Early endosomal marker, rabbit monoclonal EEA-1, was obtained from Abcam. The secondary antibody for EEA-1, Alexa Fluor 488 goat anti-rabbit antibody, was purchased from Invitrogen.

Cell Line and Cell Culture.

Human cervical cancer HeLa and the adherent human neuroblastoma IMR-32 cell lines were procured from the ATCC. 3T3-L1 fibroblast cells were a generous gift from Prof. Cliff A. Baile, Center for Animal & Dairy Science, University of Georgia. HeLa, IMR-32, and 3T3-L1 cells were grown at 37 °C in 5% CO_2 in DMEM medium supplemented with 10% fetal bovine serum and 1% penicillin/streptomycin. Cells were passed every 3 to 4 days and restarted from frozen stocks upon reaching pass number 20.

Fluorescence Imaging.

HeLa cells were seeded on microscope coverslips (1.0 cm) at a density of 6 x 10^7 cells/mL and grown overnight in DMEM. The medium was changed and fluorescent targeted and non targeted NPs were added to a final QD concentration of 10 μM. The cells were incubated for 4 h at 37 °C in 5% CO_2. MitoTracker Green (100 nM) was added and incubated for 45 min at 37 °C. The medium was removed and the cells were fixed using cold methanol for 30 min. The coverslips were then rinsed with PBS, water, and mounted on slides using mounting media. Images were collected at 320 ms for the FITC and Cy5 channels. In order to determine NP accumulation in the lysosomes of cells, HeLa cells were seeded on microscope coverslips (1.0 cm) at a density of 6 x 10^7 cells/mL and grown overnight in DMEM. The medium was changed and CelLight© Lysosome-GFP *BacMam* 2.0 was added at a concentration of 1.0 μL/10,000 cells and incubated for 24 h at 37 °C under 5% CO_2. The media was replaced and the NPs were added and allowed to internalize for varying times (1 h, 4 h, and 6 h). The medium was removed and the cells were fixed using cold methanol for 30 min. The coverslips were rinsed with PBS, water, and mounted on slides using mounting media. Images were collected at 320 ms for the FITC and Cy5 channels. Images were further analyzed with ImageJ.

Endocytosis of Targeted and non targeted-QD-blended NPs.

HeLa cells were seeded on microscope coverslips (1.0 cm) at a confluence of 1×10^6 cells per coverslip and grown overnight in a humidified incubator with 5% CO_2 at 37 °C in DMEM. The medium was changed and suspensions targeted and non targeted QD-blended NPs (0.05 mg/mL) were added. The cells were incubated for 1.0, 2.0, and 4.0 h at 37 °C. The medium was removed and the cells were fixed using 4%

paraformaldehyde at room temperature. The cells were washed three times with PBS (pH 7.4). The cells were then permeabilized with 0.1% Triton-X 100 in PBS for 10 min followed by five washes using PBS. The cells were then blocked with blocking buffer (PBS, 0.1% goat serum, 0.075% glycin) for 1 h at room temperature. The cells were incubated for 1 h at 37 °C with the early endosomal marker, rabbit polyclonal EEA-1, in a humidified box according to the manufacturer-recommended procedure. After two washes with PBS, the cells were blocked with blocking buffer for 30 min min at RT and then incubated with the secondary Alexa Fluor 488 goat anti-rabbit antibody for 1 h at 37 °C. After five washes with blocking buffer, the the cells were incubated with Hoescht 33258 for 10 min at room temperature. After five washes with PBS and three washes with water, cells were mounted on microscope slides using the mounting solution [20 mM Tris (pH 8.0), 0.5% N-propyl gallate, and 70% glycerol] for imaging. Images were collected at 320 msec for DAPI, FITC, and rhodamine channels.

Assessment of Immune Response by ELISA.

RAW macrophages were plated at a density of 2,000 cells/well and allowed to grow overnight. Cells were treated with NPs (0.5 mg/mL) and incubated for 12 h. As controls, RAW cells were left untreated or incubated with 0.125 mg/mL of LPS. An ELISA assay was performed against the cytokines IL-6 and TNF-*α* according to the manufacture's protocol. Briefly, the cell lysate was incubated in antibody-coated plates for 2 h at RT, incubated with the cytokine-biotin conjugate and streptavidin working solution. The stabilized chromagen was added to each well followed by a stop solution and the absorbance was recorded at 450 nm.

MTT Assay.

The cytotoxic behavior of all the NPs loaded with LND and *α*-TOS, was evaluated using the MTT assay against HeLa cells. Cells (2000 cells/well) were seeded on a 96-well plate in 200 *μ*L of DMEM medium and incubated for 24 h. The cells were treated with empty NPs, targeted and non targeted NPs containing the chemotherapeutics, and the free drug at varying concentrations (with respect to LND or *α*-TOS) and incubated for 12 h at 37 °C. The medium was changed, and the cells were incubated for additional 60 h. The cells were then treated with 20 *μ*L of MTT (5 mg/mL in PBS) for 5 h. The medium was removed, the cells were lysed with 100 *μ*L of DMSO, and the absorbance of the purple formazan was recorded at 550 nm. Each well was performed in triplicate. All experiments were repeated three times (Table S4). Cytotoxicity data (where appropriate) was fitted to a sigmoidal curve and a three parameters logistic model used to calculate the IC_{50}. The IC_{50} values were reported at ±95% confidence intervals. This analysis was performed with Graph Pad Prism (San Diego, U.S.A). For protective activity against neuroblastoma, IMR-32 cells were treated with 20 μM Aβ with/without different concentrations of targeted or non targeted NPs containing curcumin or free curcumin (with respect to curcumin), incubated for 12 h at 37 °C, and MTT assay was performed.

Table S1. Examples of Nanocarriers Mitochondrial Delivery.

Nanocarrier	Size (nm)	Disease	Action	References
STPP-functionalized liposomes	55	Cancer	Apoptosis	Boddapati et al. 2008. Organelle targeted nanocarriers: specific delivery of liposomal ceramide to mitochondria enhances its cytotoxicity in vitro and in vivo. Nano Lett. 8, 2559–2563.
STPP functionalized liposomes	105	Cancer	Apoptosis	Patel et al. 2010. Mitochondria-targeted liposomes improve the apoptotic and cytotoxic action of sclareol. J. Liposome Res. 20, 244–249.
Chitosan functionalized Au nanoparticles	6–16	Oxidative stress	Antioxidant	Esumi et al. 2003. Antioxidant-potentiality of gold-chitosan nanocomposites. Colloids Surf. B Biointerfaces 32, 117–123.
PAMAM functionalized Au nanoparticles	3.6	Oxidative stress	Antioxidant	Esumi et al. 2004. Antioxidant action by gold-PAMAM dendrimer nanocomposites. Langmuir 20, 2536–2538.
CTAB functionalized Au nanorods	55 × 13	Cancer	Apoptosis	Wang et al. 2011. Selective targeting of gold nanorods at the mitochondria of cancer cells: implications for cancer therapy. Nano Lett. 11, 772–780.
Oligonucleotide functionalized TiO_2 nanoparticles	3–5	Mitochondrial DNA diseases	Gene delivery	Paunesku et al. 2007. Intracellular distribution of TiO2-DNA oligonucleotide nanoconjugates directed to nucleolus and mitochondria indicates sequence specificity. Nano Lett. 7, 596–601.
Pectin functionalized Pt nanoparticles	5	Diseases with NADH dehydrogenase deficiency	Antioxidant	Hikosaka et al. 2008. Platinum nanoparticles have an activity similar to mitochondrial NADH:ubiquinone oxidoreductase. Colloids Surf. B Biointerfaces 66, 195–200.
Au/Pt bimetallic nanoparticles	5	Oxidative stress	Antioxidant	Kajita et al. 2007. Platinum nanoparticle is a useful scavenger of superoxide anion and hydrogen peroxide. Free Radic. Res. 41, 615–626.
PCL-PEG Polymeric nanoparticles	40	Oxidative stress	Antioxidant	Sharma et al. 2012. Design and Evaluation of Multifunctional Nanocarriers for Selective Delivery of Coenzyme Q10 to Mitochondria. Biomacromolecules 13, 239−252

Abbreviations: stearyl triphenyl phosphonium (STPP), polyamidoamine (PAMAM), and cetytrimethylamonium bromide (CTAB), polycaprolactone (PCL)

Table S2. Size and Zeta Potential Variation from Three Independent NP Synthesis.

	Diameter (nm)	PDI	Zeta Potential (mV)
100% PLGA-*b*-PEG-TPP NPs			
Experiment 1	84.9 ± 0.1	0.187	34.5 ± 0.6
Experiment 2	84.4 ± 0.8	0.186	32.2 ± 1.6
Experiment 3	71.9 ± 1.4	0.299	30.7 ± 2.6
90% PLGA-*b*-PEG-TPP/10% PLGA-*b*-PEG-OH NPs			
Experiment 1	84.0 ± 0.3	0.192	26.0 ± 0.5
Experiment 2	79.8 ± 1.3	0.181	27.1 ± 2.6
Experiment 3	79.1 ± 0.4	0.216	22.0 ± 1.3
80% PLGA-*b*-PEG-TPP/20% PLGA-*b*-PEG-OH NPs			
Experiment 1	83.9 ± 0.3	0.197	24.3 ± 0.9
Experiment 2	79.9 ± 0.6	0.169	22.6 ± 4.2
Experiment 3	79.4 ± 0.6	0.159	18.9 ± 1.2
65% PLGA-*b*-PEG-TPP/35% PLGA-*b*-PEG-OH			
Experiment 1	84.0 ± 0.3	0.198	22.5 ± 0.7
Experiment 2	79.4 ± 0.2	0.187	13.7 ± 0.8
Experiment 3	79.0 ± 1.5	0.199	12.4 ± 0.9
50% PLGA-*b*-PEG-TPP/50% PLGA-*b*-PEG-OH NPs			
Experiment 1	83.6 ± 0.5	0.209	7.1 ± 0.4
Experiment 2	79.6 ± 0.9	0.174	3.6 ± 0.7
Experiment 3	79.1 ± 1.1	0.237	3.6 ± 0.7
35% PLGA-*b*-PEG-TPP/65% PLGA-*b*-PEG-OH NPs			
Experiment 1	83.5 ± 0.6	0.193	1.3 ± 0.8
Experiment 2	68.9 ± 0.4	0.377	-1.2 ± 1.4
Experiment 3	65.1 ± 0.8	0.211	-0.5 ± 1.0
15% PLGA-*b*-PEG-TPP/85% PLGA-*b*-PEG-OH NPs			
Experiment 1	83.4 ± 0.7	0.195	-12.0 ± 2.9
Experiment 2	79.5 ± 0.5	0.177	-30.3 ± 0.6
Experiment 3	78.4 ± 1.7	0.232	-24.4 ± 0.8

PLGA-*b*-PEG-OH NPs			
Experiment 1	72.5 ± 0.5	0.214	-23.7 ± 0.9
Experiment 2	79.9 ± 0.5	0.191	-31.9 ± 2.4
Experiment 3	79.4 ± 0.2	0.402	-31.0 ± 0.6
90% PLGA-*b*-PEG-TPP/10% PLGA-COOH NPs			
Experiment 1	102.6 ± 1.7	0.289	30.4 ± 0.7
Experiment 2	106.7 ± 1.9	0.251	28.2 ± 1.5
Experiment 3	105.8 ± 1.6	0.291	32.1 ± 4.1
80% PLGA-*b*-PEG-TPP/20% PLGA-COOH NPs			
Experiment 1	171.0 ± 9.6	0.317	30.9 ± 0.8
Experiment 2	171.6 ± 1.9	0.286	30.6 ± 1.1
Experiment 3	176.9 ± 1.1	0.214	33.4 ± 2.2
65% PLGA-*b*-PEG-TPP/35% PLGA-COOH NPs			
Experiment 1	188.3 ± 5.7	0.270	30.9 ± 1.4
Experiment 2	189.9 ± 2.4	0.262	29.1 ± 0.5
Experiment 3	196.7 ± 4.0	0.267	32.6 ± 2.9
50% PLGA-*b*-PEG-TPP/50% PLGA-COOH NPs			
Experiment 1	212.4 ± 1.3	0.268	30.4 ± 2.8
Experiment 2	219.6 ± 4.6	0.222	27.2 ± 2.5
Experiment 3	217.2 ± 2.6	0.228	31.4 ± 4.1
35% PLGA-*b*-PEG-TPP/65% PLGA-COOH NPs			
Experiment 1	320.5 ± 0.3	0.106	30.9 ± 1.6
Experiment 2	321.2 ± 3.2	0.317	29.3 ± 2.0
Experiment 3	334.7 ± 2.1	0.334	31.9 ± 4.4
10% PLGA-*b*-PEG-TPP/90% PLGA-*b*-PEG-OH NPs			
Experiment 1	409.4 ± 2.3	0.356	31.7 ± 1.7
Experiment 2	413.7 ± 2.0	0.125	29.9 ± 2.0
Experiment 3	412.6 ± 0.7	0.108	28.1 ± 1.4

Table S3. Loading efficiencies of therapeutics at various added weight percentage.		
% wt of Therapeutics	Loading (%)	Encapsulation Efficiency (%)
Targeted-curcumin-NPs		
5	3	81
10	8	83
20	14	78
30	18	64
Non targeted-Curcumin-NPs		
5	4	83
10	9	87
20	13	75
30	18	65
Targeted-LND-NPs		
5	4	84
10	7	78
20	13	74
30	20	67
Non targeted-LND-NPs		
5	4	83
10	7	75
20	14	77
30	19	65
Targeted-*α*-TOS-NPs		
5	6	85
10	9	87
20	15	71
30	20	68
Non targeted-*α*-TOS-NPs		
5	6	87
10	8	85
20	15	76
30	21	73
Targeted-DNP-NPs		
5	5	95
10	8	81
20	17	82
30	20	67
Non targeted-DNP-NPs		
5	5	93
10	7	72
20	18	92
30	20	69

Table S4. IC_{50} Values from Three Independent Experiments.			
	Targeted-LND-NPs	**Non-targeted-LND-NPs**	**Free LND**
IC_{50}	39 ± 5 nM	207± 19 nM	>1000 μM
	Targeted-*α*-TOS-NPs	**Non-targeted-*α*-TOS-NPs**	**Free *α*-TOS**
IC_{50}	75 ± 2 nM	230 ± 4 nM	381 ± 5 nM

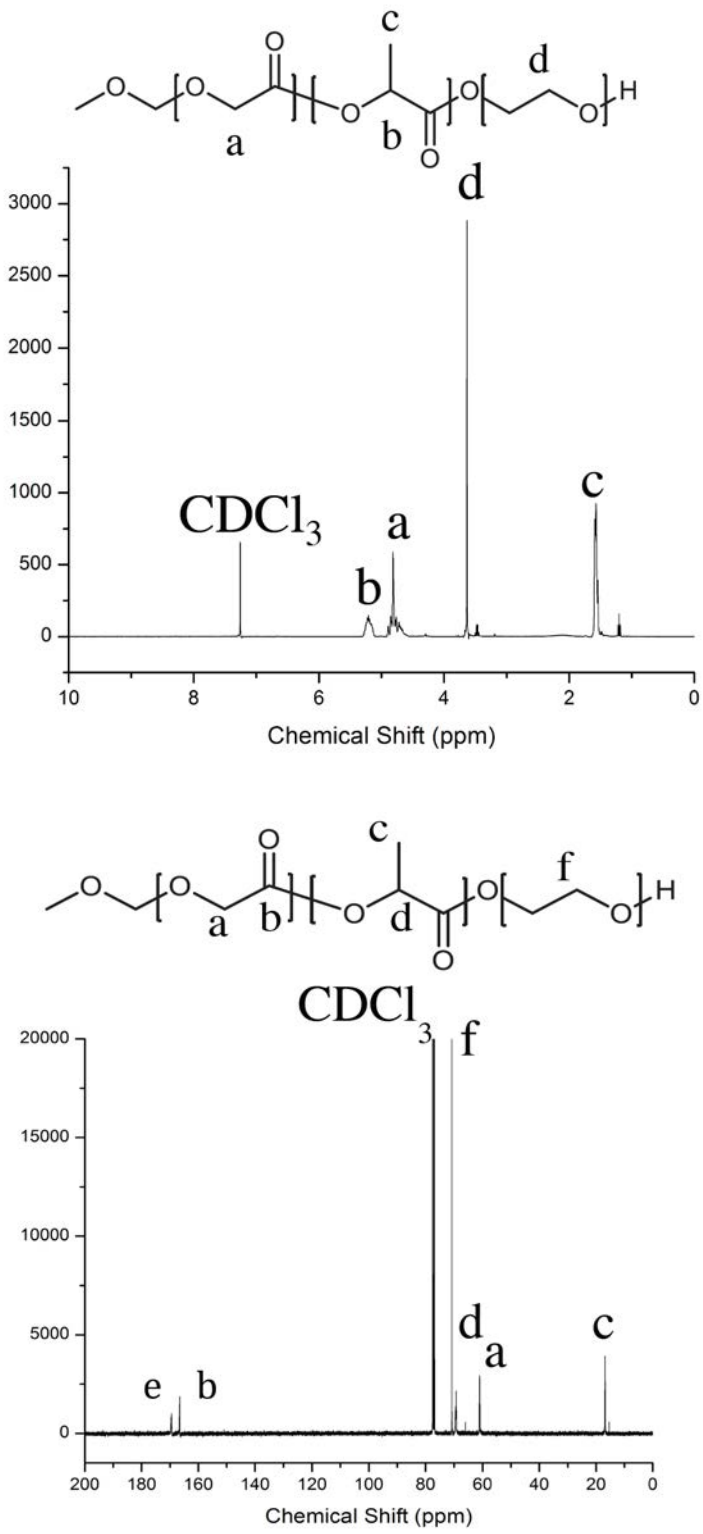

Fig. S1. ^{1}H NMR of PLGA-*b*-PEG-OH (top) and ^{13}C NMR of PLGA-*b*-PEG-OH (bottom) in $CDCl_3$.

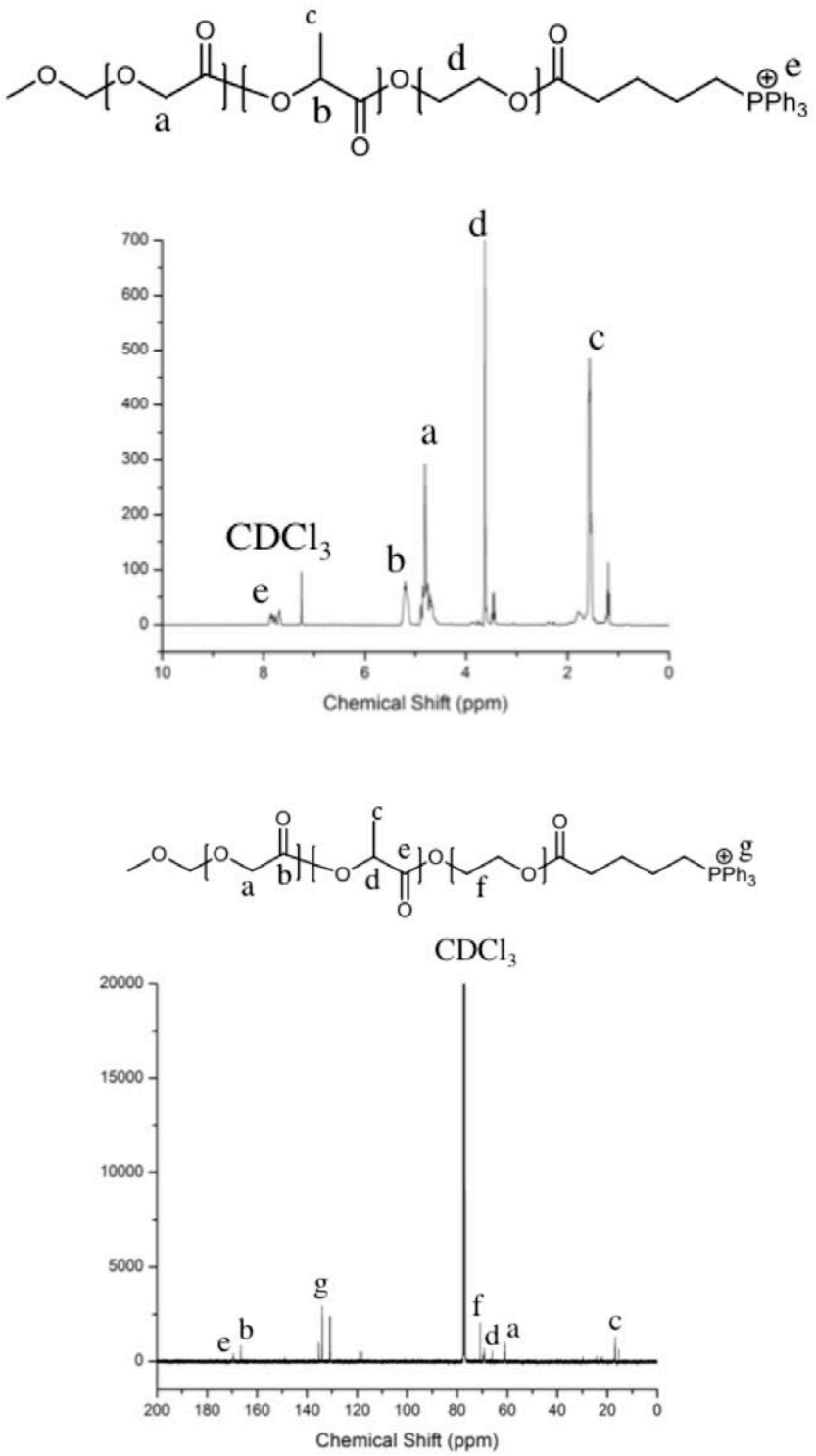

Fig. S2. ^{1}H NMR of PLGA-*b*-PEG-TPP (top) and ^{13}C NMR of PLGA-*b*-PEG-TPP (bottom) in $CDCl_3$.

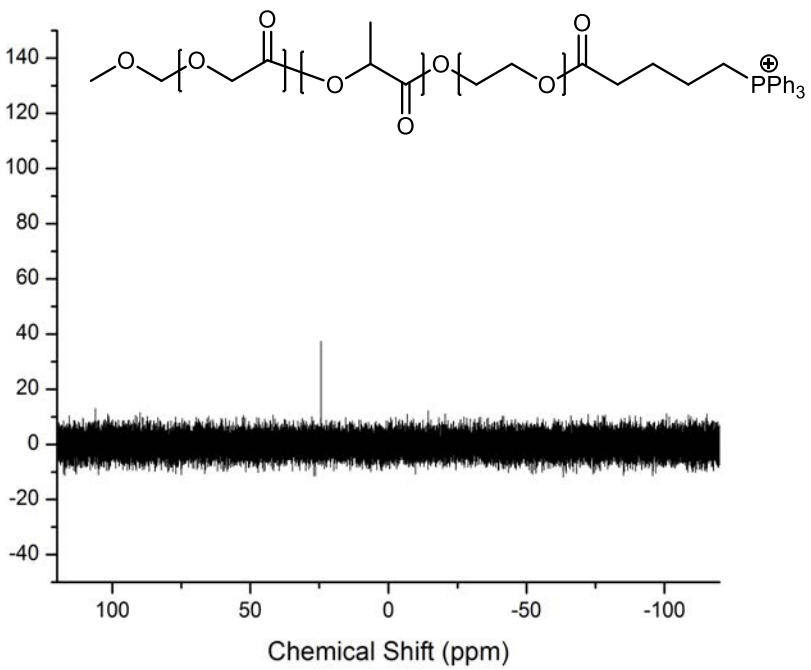

Fig. S3. ^{31}P NMR of PLGA-*b*-PEG-TPP in $CDCl_3$.

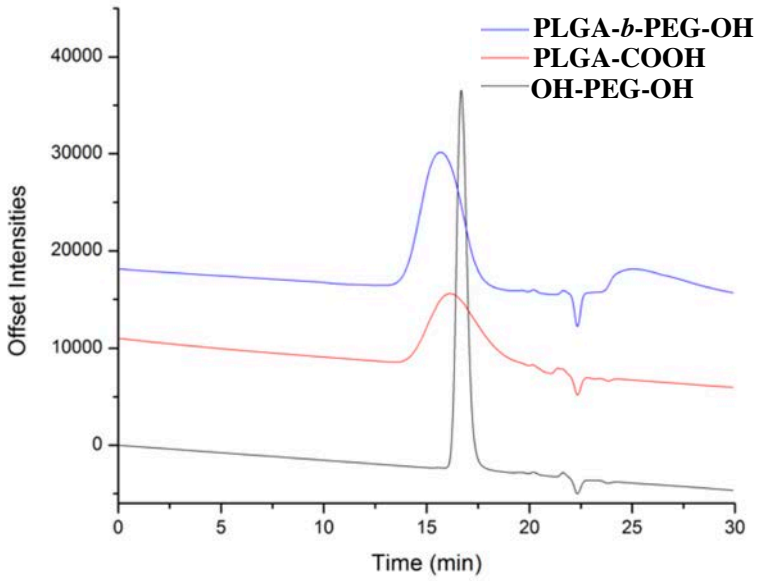

Fig. S4. Overlay of GPC traces of PLGA-*b*-PEG-OH (blue), PLGA-COOH (red), and OH-PEG-OH (MW 3350) (black) in THF at 40 °C.

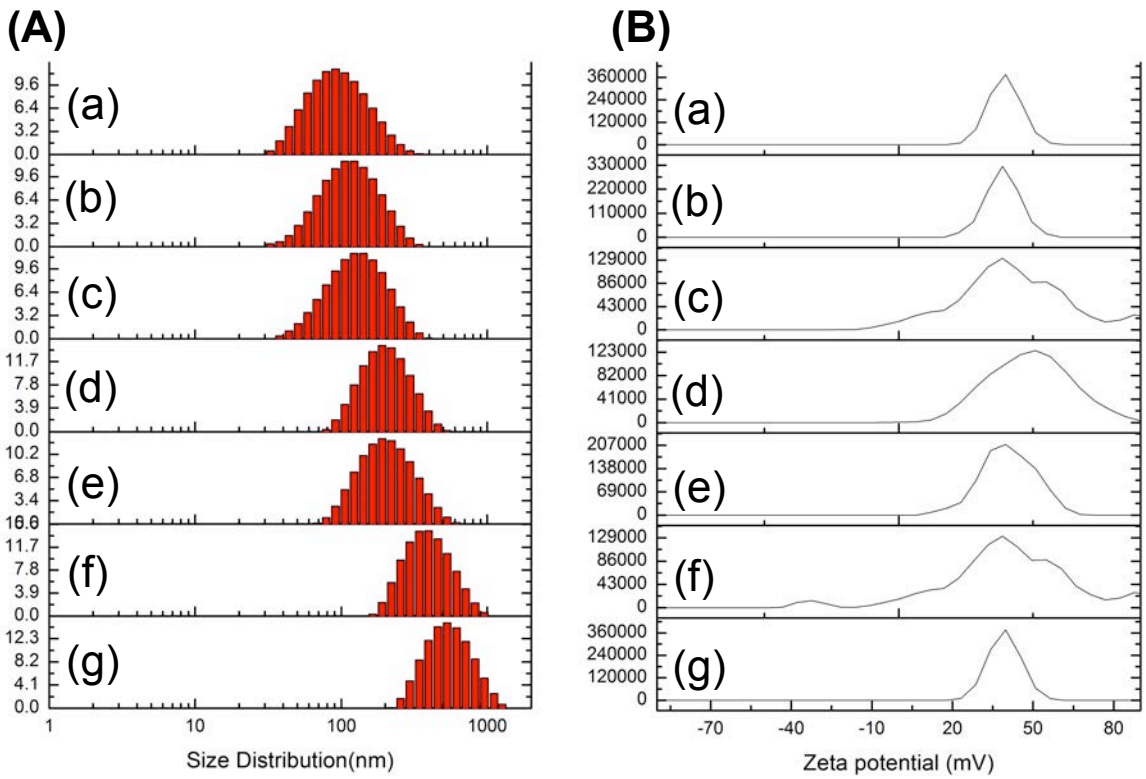

Fig. S5. Size Distribution (A) and zeta potential (B) of blended NPs with varied size: (a) 100% PLGA-*b*-PEG-TPP NPs; (b) 90% PLGA-*b*-PEG-TPP/10% PLGA-COOH NPs; (c) 80% PLGA-*b*-PEG-TPP/20% PLGA-COOH NPs; (d) 65% PLGA-*b*-PEG-TPP/35% PLGA-COOH NPs; (e) 50% PLGA-*b*-PEG-TPP/50% PLGA-COOH NPs; (f) 35% PLGA-*b*-PEG-TPP/65% PLGA-COOH NPs; and (g) 10% PLGA-*b*-PEG-TPP/90% PLGA-COOH NPs.

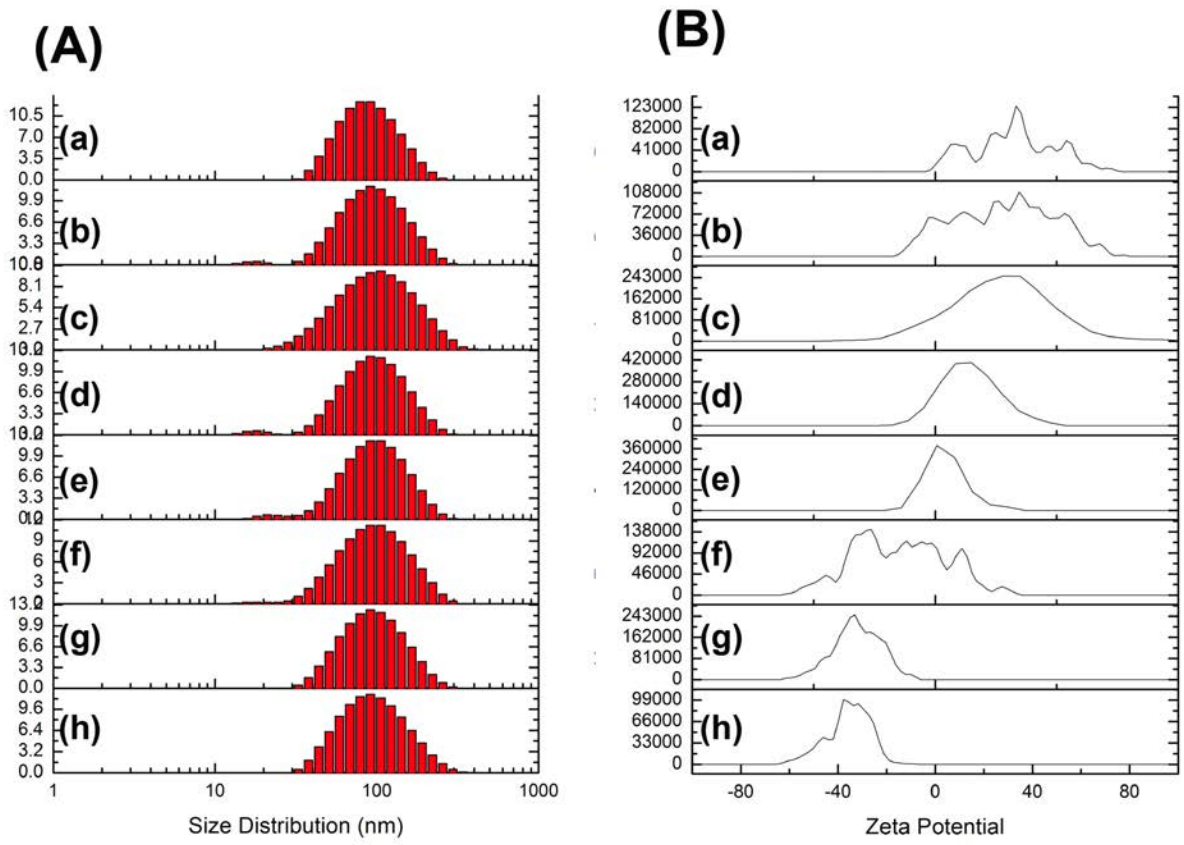

Fig. S6. Size distribution (A) and zeta potential (B) and of blended NPs with varied zeta potential: (a) 100% PLGA-*b*-PEG-TPP NPs; (b) 90% PLGA-*b*-PEG-TPP/10% PLGA-*b*-PEG-OH NPs; (c) 80% PLGA-*b*-PEG-TPP/20% PLGA-*b*-PEG-OH NPs; (d) 65% PLGA-*b*-PEG-TPP/35% PLGA-*b*-PEG-OH NPs; (e) 50% PLGA-*b*-PEG-TPP/50% PLGA-*b*-PEG-OH NPs; (f) 35% PLGA-*b*-PEG-TPP/65% PLGA-*b*-PEG-OH NPs; and (g) 15% PLGA-*b*-PEG-TPP/85% PLGA-*b*-PEG-OH NPs; (h) 100% PLGA-*b*-PEG-OH NPs.

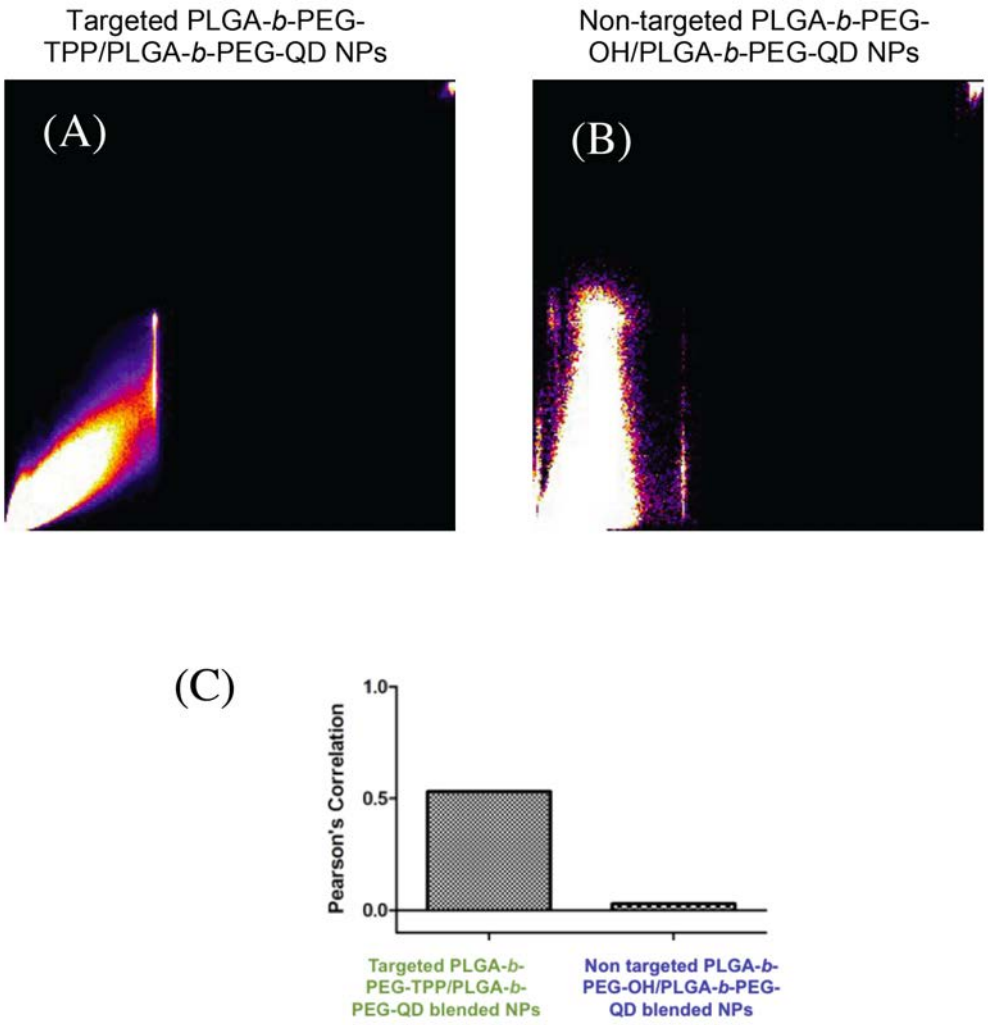

Fig. S7. (A) Colocalization Scatter Plot for targeted PLGA-*b*-PEG-TPP/PLGA-*b*-PEG-QD-blended NPs; (B) Colocalization Scatter Plot for non-targeted PLGA-*b*-PEG-OH/PLGA-*b*-PEG-QD-blended NPs; and (C) Comparison of calculated Pearson's Product Moment Correlation for (A) Colocalization Scatter Plot for targeted PLGA-*b*-PEG-TPP/PLGA-*b*-QD and non-targeted PLGA-*b*-PEG-OH/PLGA-*b*-PEG-QD-blended NPs.

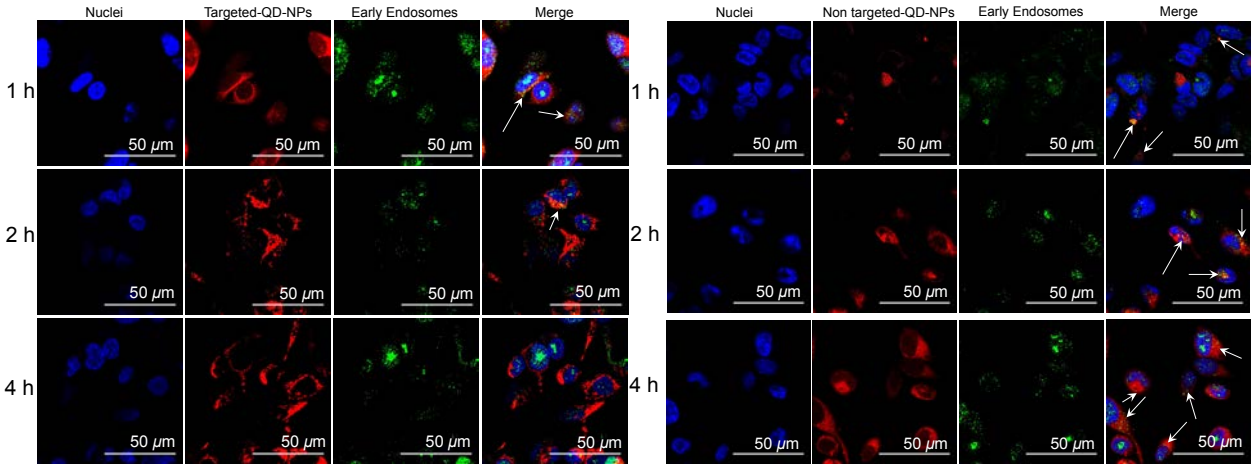

Fig. S8. Time dependent Subcellular localization of red fluorescent-targeted PLGA-*b*-PEG-TPP/PLGA-*b*-PEG-QD and non targeted PLGA-*b*-PEG-OH/PLGA-*b*-PEG-QD blended NPs in HeLa cells. The early endosomes were visualized in green by using the early endosome marker EEA-1. Co-localization with the endosomes are represented by white arrows.

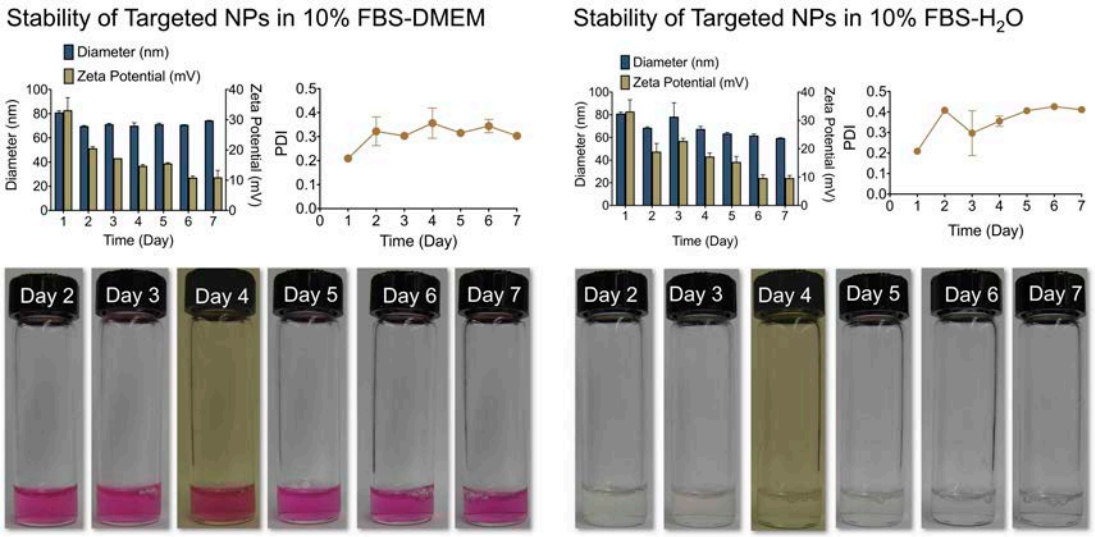

Fig. S9. Stability of targeted PLGA-*b*-PEG-TPP-NPs (5 mg/mL) in 10% FBS-DMEM (left) and 10% FBS-H_2O (right) for 7 days at 4 °C.

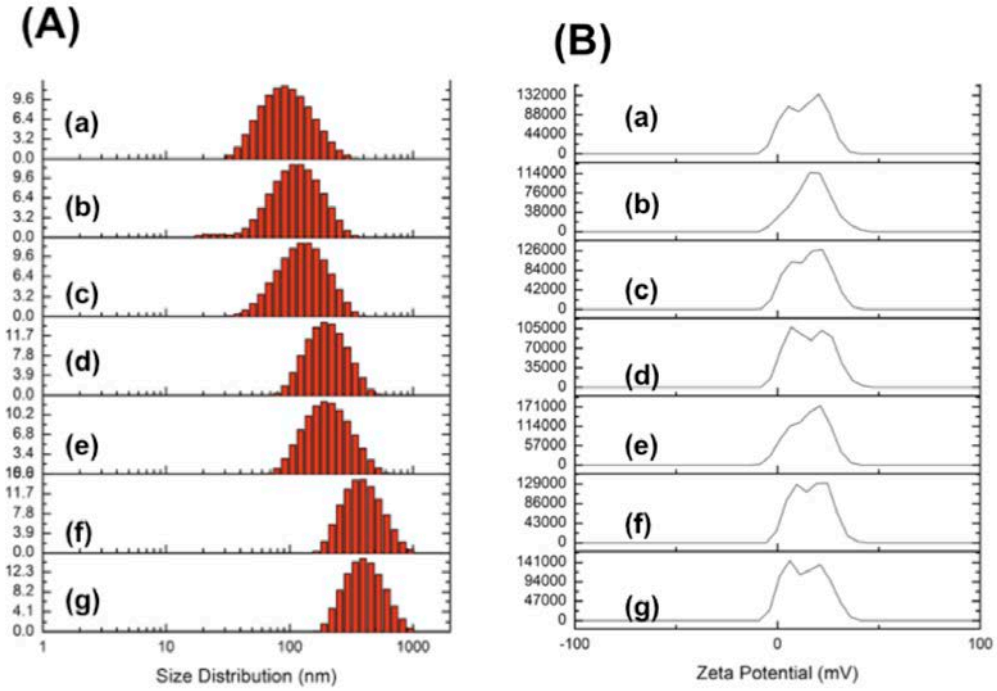

Fig. S10. Size distribution (A) and zeta potential (B) of QD-blended NPs with varied size: (a) 95% PLGA-*b*-PEG-TPP, 5% PLGA-*b*-PEG-QD NPs; (b) 87.5% PLGA-*b*-PEG-TPP/7.5% PLGA-COOH/5% PLGA-*b*-PEG-QD NPs; (c) 77.5% PLGA-*b*-PEG-TPP/17.5% PLGA-COOH/5% PLGA-*b*-PEG-QD NPs; (d) 62.5% PLGA-*b*-PEG-TPP/32.5% PLGA-COOH/5% PLGA-*b*-PEG-QD NPs; (e) 47.5% PLGA-*b*-PEG-TPP/47.5% PLGA-COOH NPs/5% PLGA-*b*-PEG-QD NPs; (f) 32.5% PLGA-*b*-PEG-TPP/62.5% PLGA-COOH/5% PLGA-*b*-PEG-QD NPs; and (g) 7.5% PLGA-*b*-PEG-TPP/92.5% PLGA-COOH/5% PLGA-*b*-PEG-QD NPs.

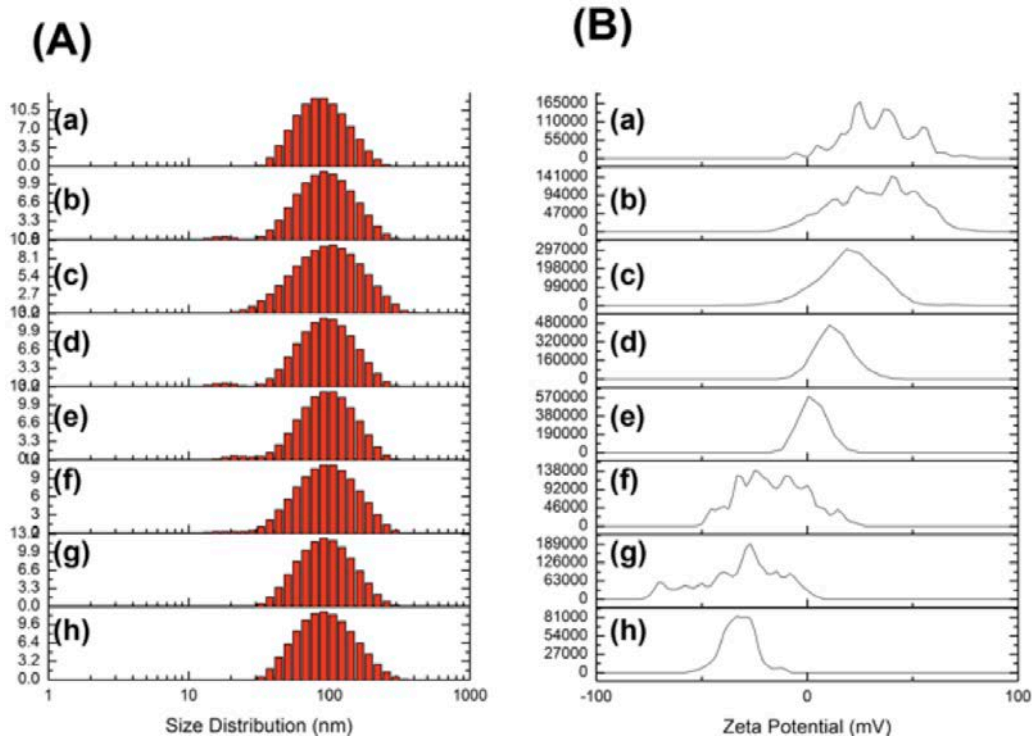

Fig. S11. Size Distribution (A) and zeta potential (B) of QD-blended NPs with varied zeta potential: (a) 95% PLGA-*b*-PEG-TPP/5% PLGA-*b*-PEG-QD NPs; (b) 87.5% PLGA-*b*-PEG-TPP/7.5% PLGA-*b*-PEG-OH/5% PLGA-*b*-PEG-QD NPs; (c) 77.5% PLGA-*b*-PEG-TPP/17.5% PLGA-*b*-PEG-OH/5% PLGA-*b*-PEG-QD NPs; (d) 62.5% PLGA-*b*-PEG-TPP/32.5% PLGA-*b*-PEG-OH/5% PLGA-*b*-PEG-QD NPs; (e) 47.5% PLGA-*b*-PEG-TPP/47.5% PLGA-*b*-PEG-OH/5% PLGA-*b*-PEG-QD NPs; (f) 32.5% PLGA-*b*-PEG-TPP/62.5% PLGA-*b*-PEG-OH/5% PLGA-*b*-PEG-QD NPs; and (g) 12.5% PLGA-*b*-PEG-TPP/82.5% PLGA-*b*-PEG-OH/5% PLGA-*b*-PEG-QD NPs; (h) 95% PLGA-*b*-PEG-OH/5% PLGA-*b*-PEG-QD NPs.

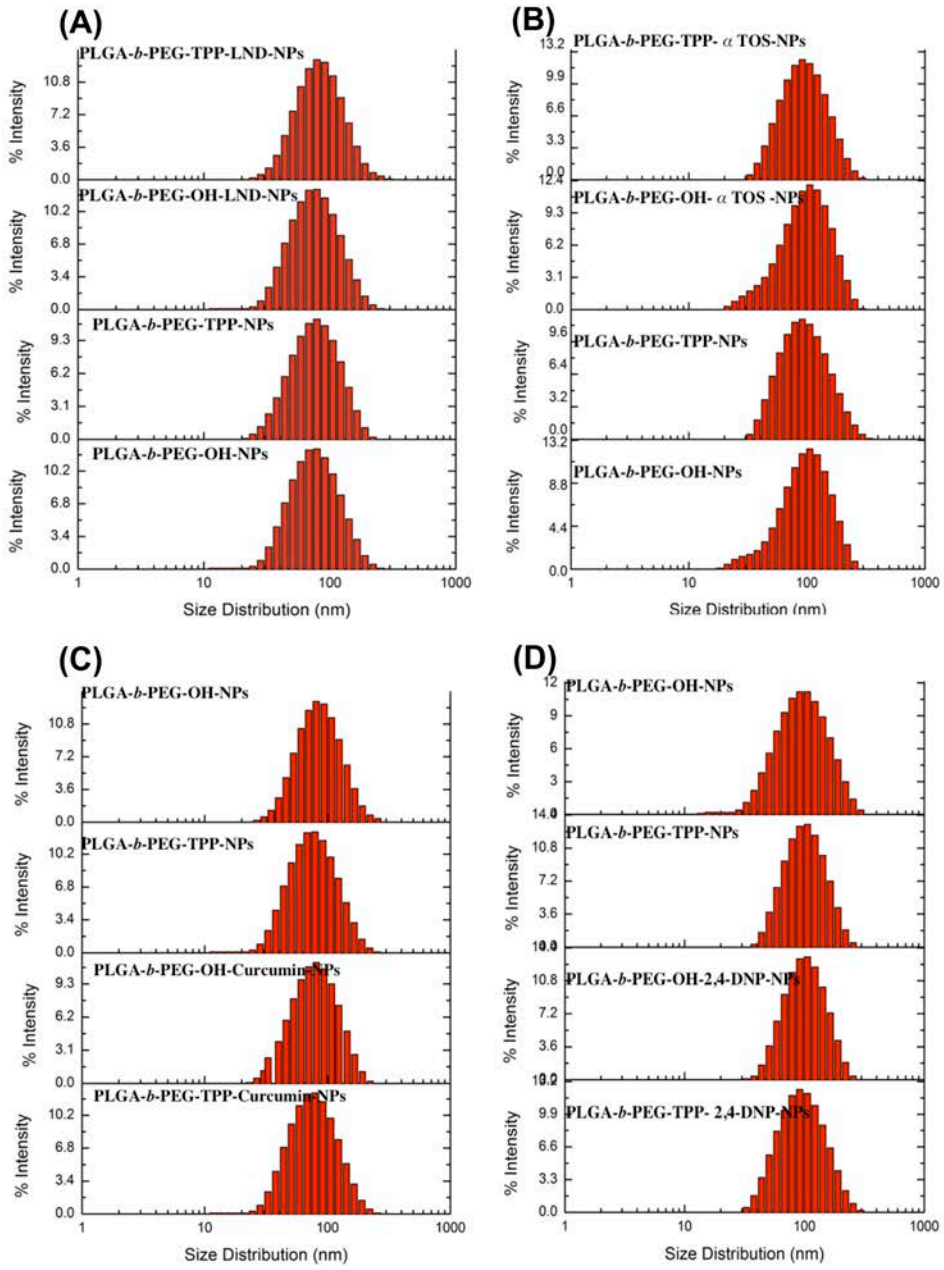

Fig. S12. (A) Size Distribution of LND loaded NPs. (B) Size Distribution of *α*-TOS loaded NPs. (C) Size Distribution of Curcumin loaded NPs. (D) Size Distribution of 2,4-DNP loaded NPs.

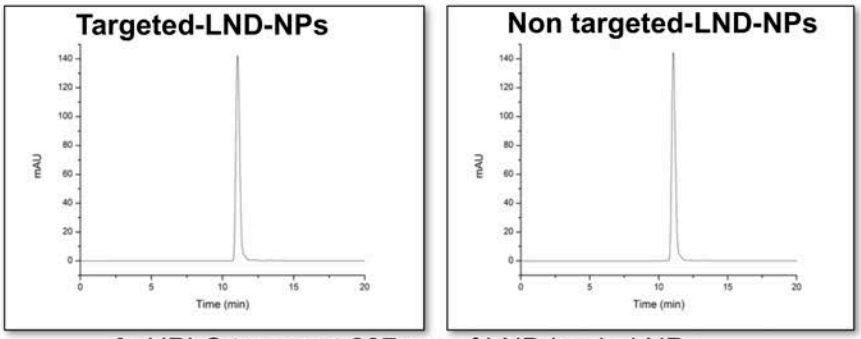

A. HPLC traces at 297 nm of LND loaded NPs.

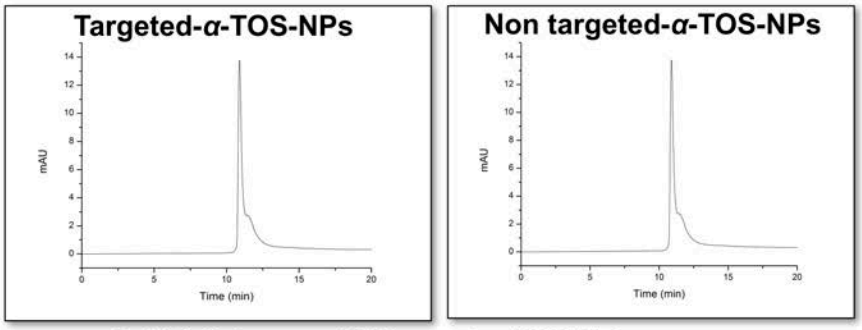

B. HPLC traces at 330 nm of *α*-TOS NPs.

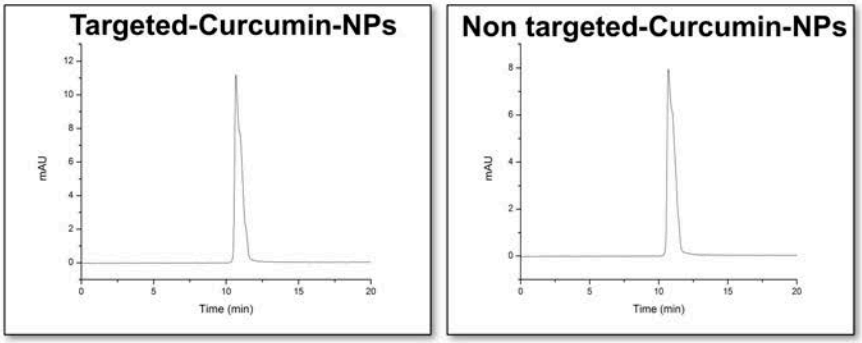

C. HPLC traces at 435 nm of curcumin loaded NPs.

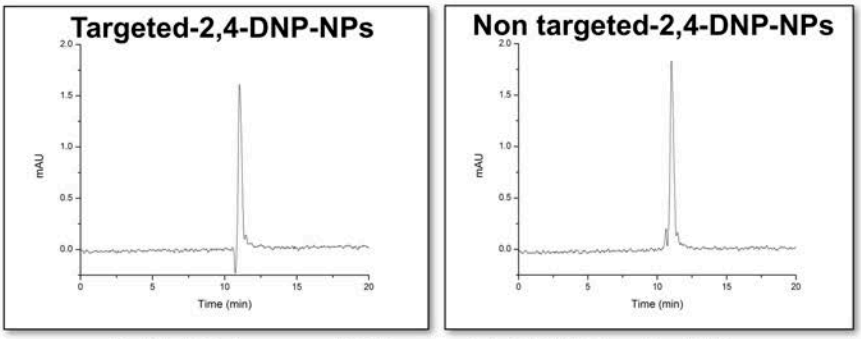

D. HPLC traces at 375 nm of 2,4 DNP loaded NPs.

Fig. S13. Representative HPLC chromatograms for quantification of drug loading and EE in therapeutics loaded NPs.

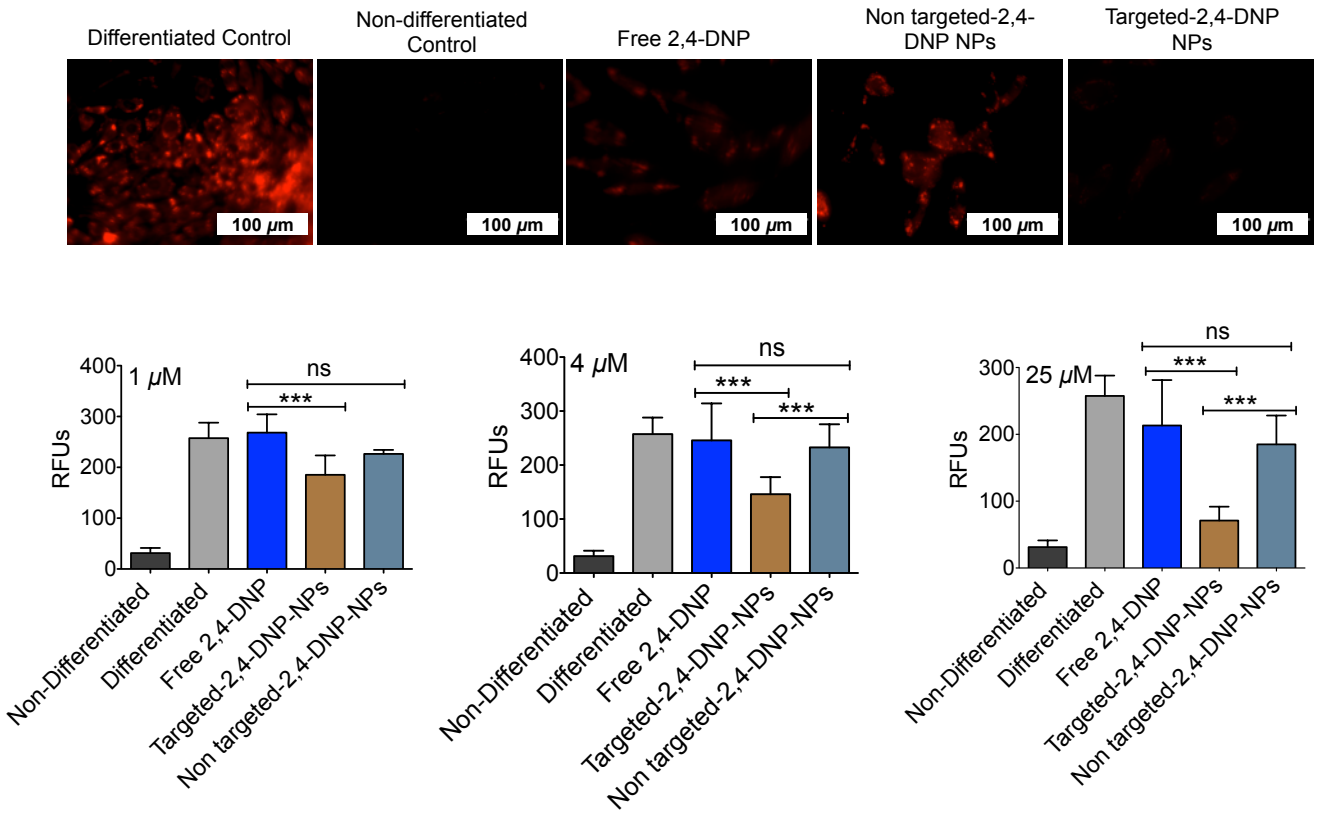

Fig. S14. Effect of targeted-2,4-DNP-NPs, non targeted-2,4-DNP-NPs, and free 2,4-DNP on adipocyte differentiation. Top: fluorescence images after 7 days, the cells were stained with Oil-red-O to visualize the degree of lipid accumulation. Bottom: quantification of stained cells using relative fluorescence intensity at different concentrations.